Title: Mutational landscape and molecular bases of echinocandin resistance

Authors: Romain Durand[1,2,3,4,5], Alexandre G. Torbey[3,6], Mathieu Giguere[1,2,3,4], Alicia Pageau[1,2,3,4,5], Alexandre K. Dubé[1,2,3,4,5], Patrick Lagüe[1,2,3*] and Christian R. Landry[1,2,3,4,5*]

Affiliations:

[1]Département de Biochimie, de Microbiologie et de Bio-informatique, Faculté des Sciences et de Génie, Université Laval; Québec, G1V 0A6, Canada.

[2]Institut de Biologie Intégrative et des Systèmes (IBIS), Université Laval; Québec, G1V 0A6, Canada.

[3]PROTEO, Le regroupement québécois de recherche sur la fonction, l'ingénierie et les applications des protéines, Université Laval; Québec, G1V 0A6, Canada.

[4]Centre de Recherche sur les Données Massives (CRDM), Université Laval; Québec, G1V 0A6, Canada.

[5]Département de Biologie, Faculté des Sciences et de Génie, Université Laval; Québec, G1V 0A6, Canada.

[6]Institut National de la Recherche Scientifique, Centre Armand-Frappier; Laval, H7V 1B7, Canada.

*Corresponding authors. Emails: patrick.lague@bcm.ulaval.ca or christian.landry@bio.ulaval.ca

Abstract: One of the front-line drug classes used to treat invasive fungal infections is echinocandins, which target the fungal-specific beta-glucan synthase (Fks). Treatment failure due to resistance often coincides with mutations in two protein regions known as hotspots. The biophysical bases by which such mutations confer resistance and cross-resistance among echinocandins are largely unknown. Here, we use deep-mutational scanning to quantify the resistance level of 660 mutations in the hotspots of two homologous Fks. We detail the constraints acting on drug binding and explain the resistance specificity for some mutations using the drug-protein interactions from our molecular models. Our findings will enable DNA sequence-based predictions of resistance to this important drug family and the improvement of future molecules that could overcome current resistance mutations.

One sentence summary: Disruption of specific interactions between echinocandins and key residues from their target lead to drug-specific resistance.

Main Text:

Echinocandins are arguably the most important compounds to combat human fungal infections. They are routinely used to treat invasive candidiasis and are the only recourse against the emerging pathogen *Candida auris* (*1*, *2*). Unfortunately, their efficiency is hindered by the acquisition of resistance, which occurs mostly through mutations in the drug target: the β-1,3-glucan synthase Fks1 (*3*). Mutations reported to correlate with treatment failure are concentrated in two regions of the coding sequence, which have hence been referred to as "hotspots" (*4*, *5*). Despite the importance of echinocandins and the growing threat of resistant pathogens, very little is known regarding the molecular mechanisms at play. The drugs are hypothesized to act as non-competitive inhibitors of the enzyme, although their exact mechanism of action is still unclear (*6*). The correlation between treatment failure and amino acid changes in the hotspots has led to the hypothesis that echinocandins bind these two regions. However, this association remains to be supported with biophysical data. The structure of Fks1 from the budding yeast *Saccharomyces cerevisiae* has recently been solved by cryo-electron microscopy (Fig. 1A) (*7*), which has led to the observation that binding of echinocandins in the spatially close hotspots is favorable using molecular docking (*8*). While these recent advances have been insufficient to characterize the exact mechanisms leading to resistance, there is little doubt that the missing piece of the puzzle lies in the hotspots. Elucidating these mechanisms would be key for predicting resistance from hotspot sequences alone and explaining the extent and nature of cross-resistance among drugs within the echinocandin family. Additionally, detailed drug-binding models could be exploited in the future to guide the design of therapeutics.

In this study, we exploit the structure of Fks1 to improve our understanding of resistance at the biophysical level. We first use deep-mutational scanning (DMS) to generate all possible single mutants of each hotspot for both Fks genes present in *S. cerevisiae* (paralogs from the ancestral whole-genome duplication). All mutants were screened using the three most widely used echinocandins in clinical settings: caspofungin, micafungin and anidulafungin. We show that this data allows for machine-learning assisted predictions of resistance. Secondly, we performed molecular docking using 3D free energy maps obtained from Site Identification by Ligand Competitive Saturation (SILCS) (*9*) to predict the binding of each drug to Fks1. We show which molecular interactions ensure drug-specific binding and how mutations lead to cross-resistance or drug-specific resistance.

Deep-mutational scanning of the putative binding sites of echinocandins

Deep-mutational scanning was performed independently on the two hotspots of *FKS1* and *FKS2* in the genome of *S. cerevisiae*. The two genes are partly redundant (*10*), which allows editing them individually directly in the genome. Some fungi have only one ortholog of these genes, but two are often present, for instance, in the closely related pathogen *N. glabratus* (fig. S1). Studying both genes allows us to capture potential differences in the impact of mutations. Furthermore, the main paralog Fks1 of *S. cerevisiae* is the one for which the structure was recently solved by cryo-electron microscopy (Fig. 1A).

Mutant oligo libraries (NNK codon at each position) were amplified and integrated at the endogenous hotspot loci using CRISPR-Cas9 (Fig. 1B). These mutant strains were cultured overnight without selective pressure. They were then exposed to the three echinocandins (anidulafungin, caspofungin, micafungin). The concentrations used were estimated to inhibit around 80% of wild-type growth. Cells were harvested before and after selection and the

genomic loci corresponding to the two hotspots were sequenced to estimate the extent of selection acting on each variant.

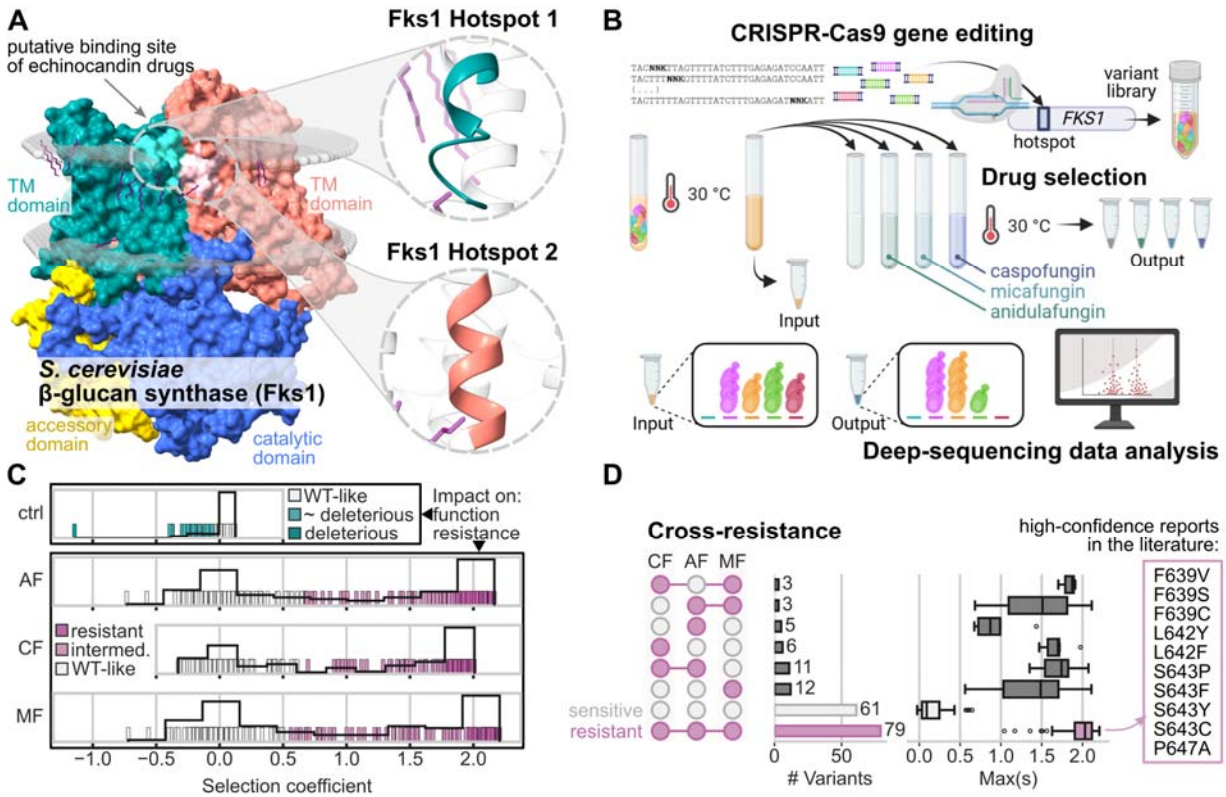

Fig. 1. Deep-mutational scanning of β-glucan synthase (Fks) hotspots identifies specific and cross-resistance mutations to echinocandins. (**A**) Hotspots 1 and 2 on Fks1 (PDB: 7XE4) (*7*), visualized using UCSF ChimeraX (*27*). Individual domains are colored. The approximate location of membrane bilayers is shown by two semi-opaque circular planes. Lipids present in the structure are represented in purple sticks. (**B**) Experimental design for the DMS assay, created with BioRender, showing the library of single mutants (NNK) inserted in the hotspot 1 of *FKS1* as an example. (**C**) Distribution of effects for single mutants of the hotspot 1 of Fks1 (including wild-type) in each condition. In the control condition (ctrl), the effect relates to protein function, whereas in the presence of drug (AF, anidulafungin; CF, caspofungin; MF, micafungin), the effect informs on resistance. Effects were quantified using the selection coefficient (the wild-type is expected to have a selection coefficient around 0). Variants were classified based on their effect using a Gaussian mixture model. (**D**) UpSet plot showing the number of unique Fks1-HS1 amino acid sequences conferring resistance (pink circles) or being sensitive (white circles) to each drug, and their overlap. 79 single mutants are resistant to all three echinocandins. On the right, a boxplot shows the corresponding maximum selection coefficient across drugs for each set. We highlight ten resistance mutations that have previously been lab validated in other studies.

All mutants were accounted for in the initial libraries, but some were depleted during the preculture (see supplementary text section S1), potentially due to their deleteriousness. Mutating hotspot 2 in either paralog often resulted in a strong growth defect, which we hypothesize is related to its important role in stabilizing the structure within the membrane (fig. S2, more details in the following sections).

Selection coefficients were computed for each nucleotide variant and then averaged for each amino acid variant. Replicates among cultures (at the nucleotide level) are well correlated, with a Pearson's correlation coefficient above 0.9 for all but one of the drug conditions (fig. S3). Overall, we obtain a bimodal distribution of effects, regardless of the drug used (Fig. 1C), or the nature of the mutated hotspot (fig. S4). This bimodality is consistent with strong selective pressure allowing only resistant mutants to grow significantly.

Classification and validation of mutational effects

Overall, 119 out of 180 classified Fks1-HS1 mutants (66%) are resistant to at least one drug (either intermediate or resistant, Fig. 1D). Ten of these mutations have previously been reported in lab and lab-evolved strains of *S. cerevisiae*, *Candida albicans*, *N. glabratus*, *Aspergillus fumigatus*, *Clavispora lusitaniae*, *Candida parapsilosis* and *Candida metapsilosis* (S1 Data). Our results experimentally validate these observations and further show that resistance among species could be acquired through parallel evolution to the same variants. This suggests that observations made in one species are informative for predicting resistance phenotypes in other species.

One major concern with the apparition of resistance mutations in fungi is the extent of cross-resistance, since very few classes of molecules are available, with few molecules within each class (*11*). Identifying echinocandin-specific resistant mutants is important from a clinical standpoint. Indeed, if a patient is infected with a pathogen carrying one of these mutations, a recommendation could be emitted to use the drug the pathogen is predicted to be sensitive to. 79 out of 119 resistant mutants (44%) are cross-resistant to all three tested echinocandins (Fig. 1D). Twelve mutants are resistant to micafungin only, whereas eleven are resistant to caspofungin or anidulafungin, but not micafungin (Fig. 1D). We also find almost half of all classified Fks1-HS2 mutants are resistant to at least one drug, with 33 of them (57% of resistant mutants) being pan-echinocandin resistant (fig. S5). Contrasting with the resistance profile of Fks1-HS1 mutants, none of the Fks1-HS2 mutants are resistant to micafungin only. Instead, 22 mutants are resistant to anidulafungin (n=10), caspofungin (n=4) or both (n=8) (fig. S5).

In order to validate the effects of these mutations on resistance, 28 single mutants in the hotspot 1 of Fks1 were recreated by genome editing. The calculated fitness values strongly correlate with the selection coefficients from the bulk-competition assay (Spearman's r = 0.92-0.96 across drugs, p-value <= 4.4e-11, fig. S6). Interestingly, we find variants displaying an intermediate resistance phenotype for all three tested drugs, validating this observation as biologically relevant and not a byproduct of the bulk competition assay (fig. S6). In addition to missense mutations, we also attempted to introduce all possible codon deletions in the hotspot 1 of *FKS1*, as this type of mutation has previously been reported in *N. glabratus (5, 12–14)*. However, all attempts yielded no colonies, hinting at a strong fitness cost for these mutations.

Key positions in Fks1 are associated with echinocandin resistance

We identified five positions that are determinant for echinocandin resistance. Mutations at positions 639, 643, 646 and 647 cause resistance to anidulafungin and caspofungin (Fig. 2BC). In contrast, mutating positions 639, 643, 645 and 647 cause micafungin resistance (Fig. 2D). Almost all single amino acid substitutions result in drug resistance, with no fitness tradeoff (Fig. 2A-D). This confirms the crucial role of these hotspot regions in conferring resistance upon amino acid changes.

In the case of hotspot 2, many variants show a deleterious effect in the presence of echinocandin (Fig. 2E-H). Because of this strong selection, the cultures grew more slowly, reaching fewer

mitotic generations (fig. S2B) such that selection coefficients of resistant mutants are inflated (fig. S4CD). In particular, most substitutions at position 1357 confer strong pan-echinocandin resistance (Fig. 2F-H). Mutating position 1360 also causes resistance to anidulafungin and caspofungin, but not micafungin (Fig. 2F-H).

In *S. cerevisiae*, *FKS2* is normally not expressed during vegetative growth unless *FKS1* is repressed or inactivated (*10*). We therefore measured the impact of amino acid substitutions when repressing *FKS1*. As expected from synthetic lethal gene duplicates, introducing premature stop codons in *FKS2* hotspots has little effect in the WT background but results in a strongly deleterious effect when repressing *FKS1* (fig. S7). Despite a lower resolution for this gene, the data obtained for other substitutions corroborate what was obtained with Fks1 (fig. S7), which we attribute to the high percentage of protein sequence identity between both paralogs (87.7%) and their functional redundancy. More specifically, substitutions at position 662, 1376 and 1379 (homologous to S643, R1357 and L1360 in Fks1, respectively) often confer pan-echinocandin resistance, while substitutions at R664 (homologous to R645 in Fks1) cause micafungin-specific resistance (figs. S7-8).

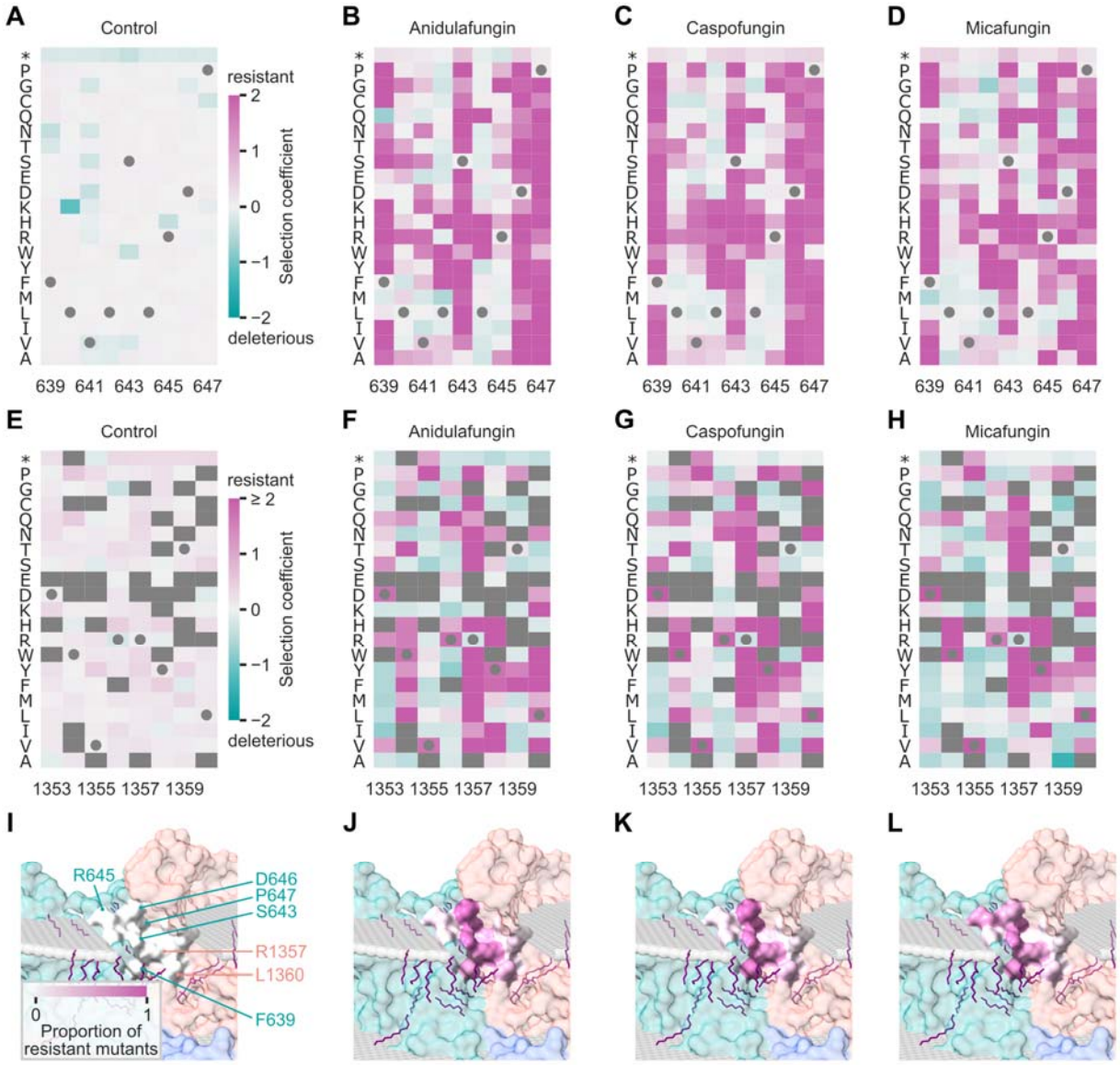

Fig. 2. Crucial positions in Fks1 for echinocandin resistance. (**A-H**) Selection coefficients (median of synonymous variants) of individual mutants in hotspots 1 (A-D) and 2 (E-H) of Fks1 in control (A, E), anidulafungin (B, F), caspofungin (C, G) and micafungin (D, H). The wild-type sequence is indicated by gray circles. We computed the selection coefficients of five mutants absent from the initial mutant libraries: F639C, L640D, L642G, P647N and P647Q in validation assays. In panels E-H, some variants have a selection coefficient above 2 but were set to 2 to ease the data representation (see the distribution of values in fig. S4). (**I-L**) For each condition (same order as previous panels), both hotspots in the structure of Fks1 are colored according to the proportion of mutants classified as resistant (see Fig. 1D) at each position (relative to the number of mutants for which we were able to obtain a selection coefficient), with key residues highlighted in the same color scheme as Fig. 1A. Lipids present in the structure (*7*) are represented in purple sticks.

The simple sequence-resistance maps allow prediction of resistance from sequences alone

The full sequence-resistance relationship we obtained from the DMS could allow the prediction of resistance from DNA sequence alone. To test this possibility, we spiked the initial libraries of single mutants with DNA fragments corresponding to 50 fungal orthologous sequences. We then use the *S. cerevisiae* sequence data to predict the sensitivity and resistance of these orthologous hotspots including those of the most important fungal pathogens (*15*), namely *C. auris*, *C. albicans*, *N. glabratus* and *Candida tropicalis*. The obtained results corroborate the known susceptibility profiles of each of these organisms (*11*). Despite these ortholog hotspots differing from *S. cerevisiae* WT by 2 to 7 residues, the model accurately predicts resistance to any of the three tested echinocandins for most sequences tested (Fig. 3A). For example, our model predicts that the hotspot 1 of the Fks ortholog encoded by the fungal pathogen *C. parapsilosis* is insensitive to all three echinocandins. This prediction is validated by our DMS data, which means the hotspot sequence alone is both sufficient and, in the native context, necessary to explain the decreased sensitivity of several *C. parapsilosis* strains (*16*). For more distant orthologs such as *Cryptococcus neoformans*'s hotspot, the hotspot sequence appears sufficient to confer decreased sensitivity, but is not actually necessary to explain the intrinsic resistance of this species to echinocandins, which is instead linked to low β-1,3-glucan content in the cell wall (*17*).

To obtain predictions on clinically relevant mutations, we ran the same trained model on a different testing set comprising hotspot 1 sequences from Fks1 or Fks2 with single amino acid substitutions previously reported in the literature (S1 Data). Again, the model accurately classified more than 86% of reported resistant hotspots (Fig. 3B). Interestingly, the model accurately predicted resistance regardless of the location of the hotspot on either paralog. Some sequences were inaccurately classified, which we attribute either to low confidence data, or to other potentially unreported factors affecting resistance phenotypes such as heterozygosity of the mutations in the clinical strains (*18*, *19*).

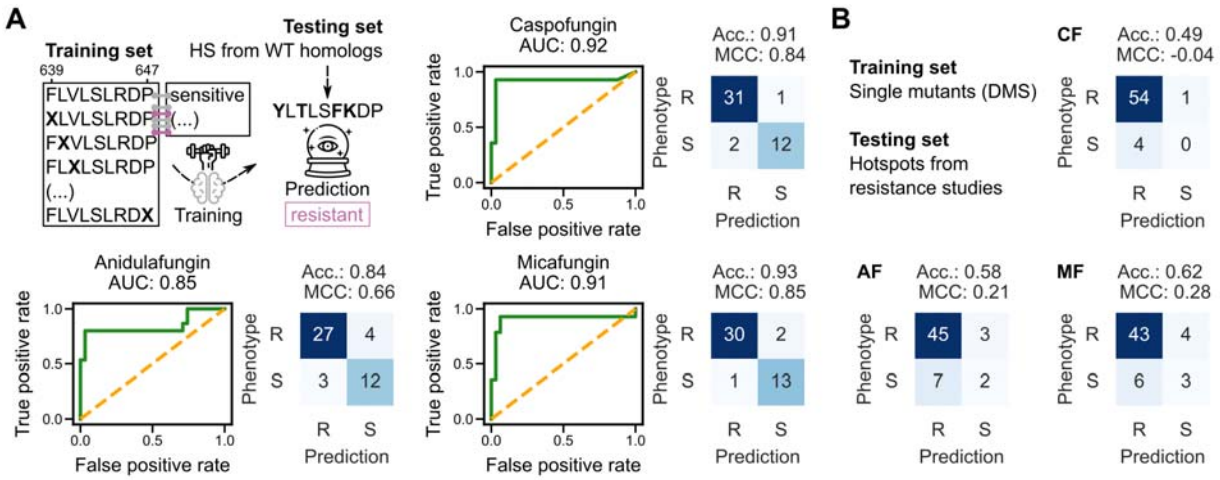

Fig. 3. Machine-learning assisted prediction of resistance. (**A**) Prediction of resistance for all Fks1-HS1 orthologous hotspots with two or more amino acid substitutions compared to *S. cerevisiae* WT. A random forest classifier was trained on all single mutants of the DMS dataset, using a combination of hotspot position and amino acid properties as features. For each drug, the AUC-ROC curve is displayed alongside the confusion matrix. Acc: balanced accuracy score, MCC: Matthew's correlation coefficient, R: resistant, S: sensitive. "Training" icon by Creative Mahira and "Crystal Ball" icon by Agus Raharjo from Noun Project (CC BY 3.0). (**B**) Prediction of resistance for Fks1-HS1 and Fks2-HS1 mutants reported in the literature, using the same model and training set as in panel A. Here, because the testing set includes few reports of sensitivity, only the confusion matrix is shown.

Echinocandins bind to solvent-exposed Fks1 hotspots

Next, we sought to characterize the molecular bases of echinocandin cross-resistance and drug-specific resistance. First, we used classical molecular dynamics (MD) simulations to equilibrate the structure of Fks1. Then, we performed SILCS-MD simulations to identify all possible binding pockets (Fig. 4A). Briefly, we used standard pharmacophoric fragments which compete for binding during the dynamic simulation. Because each of these fragments are characterized by a specific electrostatic profile, each identified pocket is specific to one atom of any fragment. The identified pockets are volumetric maps that reveal an ensemble of specific interactions that are probable in the timeframe of the simulation. For this reason, they are hereafter referred to by their technical term: FragMaps. FragMaps, with their specific properties, can represent different chemical functions carried by the drugs (table S1). For example, the generic hydrogen bond acceptor FragMap can represent the hydroxyls of all three echinocandins or the sulfate of micafungin (table S1). All FragMaps (n=14) were used to guide the molecular docking of each echinocandin, resulting in non-rigid poses that minimize the relative free energy of binding. We used these poses to infer how substitutions would affect binding, explaining resistance.

The water oxygen FragMap shows deformation in the upper leaflet of the membrane around hotspot 2 and part of hotspot 1 (Fig. 4B). This indicates that the upper part of the hotspot cavity is exposed to the extracellular solvent, while the lower part remains embedded in the lipid bilayer. This suggests that drug binding occurs in a potentially solvent-exposed environment, affecting the positioning and interaction of the drugs. It also highlights the importance of the drug's hydrophobic tail rigidity for stable binding in the hotspot cavity (*20*) (see supplementary text section S2, fig. S9).

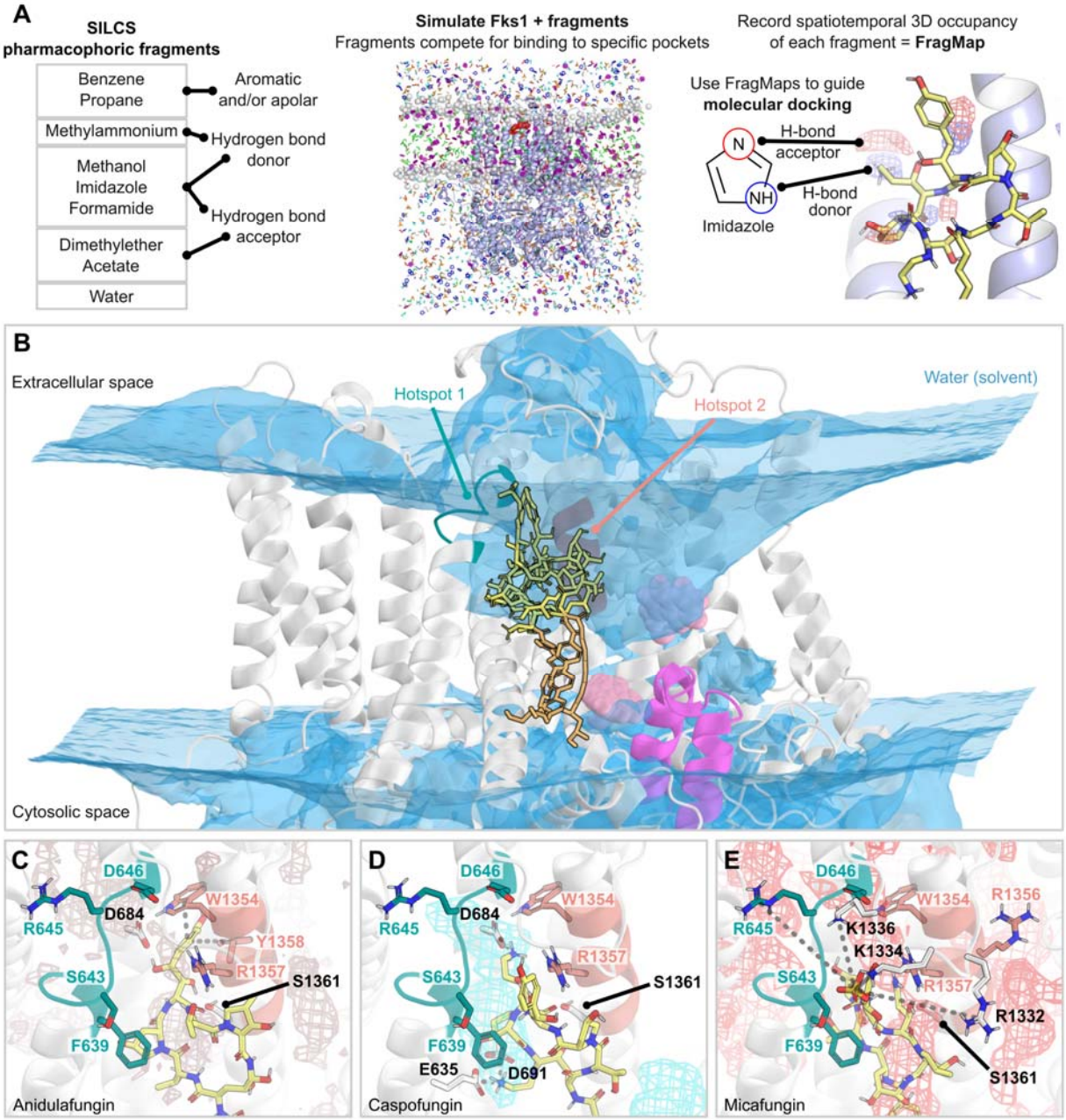

Fig. 4. Molecular bases of echinocandin binding. (**A**) Experimental design for the SILCS-MD simulations, in which pharmacophoric fragments (left) compete for binding to Fks1 (center). The obtained FragMaps were used to guide molecular docking of echinocandins. On the right, we show two FragMaps as blue and red meshes: hydrogen bond donor and hydrogen bond acceptor, respectively (two distinct imidazole nitrogen atoms). (**B**) Water oxygen FragMap (blue surface) across Fks1 (white ribbon) from SILCS simulations in the absence of echinocandin reveals solvent exposure in Fks1's transmembrane region, particularly around hotspot 2 (salmon) and part of hotspot 1 (dark cyan). This region is bordered by tryptophan residues (pink spheres) and transmembrane (TM) helices TM9-10 (magenta). The cyclic peptide cores of the three echinocandins are shown in yellow sticks, with their lipophilic tails colored orange. (**C-E**) Docking poses of anidulafungin (C), caspofungin (D) and micafungin (E) on the MD-equilibrated Fks1 structure. Atoms are colored as follows: polar hydrogen, white; carbon, yellow

(drug structures only); nitrogen, blue; oxygen, red. In each panel, the following FragMaps are represented by colored meshes: C) methanol oxygen in gray, D) methylamine nitrogen in light cyan, E) hydrogen bond donor in pale red. Analogies between FragMaps and drug chemical groups are listed in table S1. Echinocandins interact (gray dashed lines) with key hotspot residues whose side chains are colored dark cyan and salmon, respectively, as well as some residues outside the mutated hotspots (white carbons, black labels). Figures were generated using PyMOL v2.5.5 (*28*).

Drug binding is mediated through interactions with key residues both in and out of the hotspots

The three drugs align well with up to three FragMaps, highlighting both drug-specific and common dipole or hydrogen bond interactions with the echinocandins' peptide core (Figs. 4C-E). Anidulafungin, lacking strong hydrogen bond donors or acceptors (fig. S10), fits well with the methanol oxygen FragMap in the hotspot cavity due to its hydroxyl functions (Fig. 4C). The smaller size of anidulafungin compared to the two other echinocandins enables deeper docking into the hotspot cavity, with homotyrosine hydroxyls fitting near D684 and S1361, suggesting a role in binding (Fig. 4C). Additionally, anidulafungin's homotyrosine residue engages in π-stacking with W1354 and Y1358 in hotspot 2 which extends into the glucan translocation channel (figs. S11-12).

Caspofungin docks more shallowly into the hotspot cavity (Fig. 4D), likely due to steric hindrance and poor fit with FragMaps in the extracellular part of the hotspot cavity. Its flexible aliphatic tail does not contribute to binding (fig. S9). Caspofungin is also characterized by two ornithine residues (fig. S10), with terminal amides fitting within the methylamine nitrogen FragMaps near E635, D684 and D691 (Fig. 4D). All three residues are very conserved, which indicates that a mutation at these positions would be very costly and thus unlikely to contribute to resistance.

Micafungin, characterized by its sulfated dihydroxy homotyrosine and hydroxy asparagine (fig. S10), docks near basic residues close to a large hydrogen bond acceptor FragMap on the extracellular part of the hotspot cavity (Fig. 4E). The size of the FragMap indicates that micafungin is likely to penetrate deeper, which is supported by the presence of an extracellular loop covering the top of the cavity. This not only contributes substantially to drug binding but may also affect the proposed glucan translocation channel (*7*) (see supplementary text section S3, fig. S11), likely explaining why micafungin exhibits the strongest inhibitory activity out of the three tested echinocandins (*21*).

Disruption of bonds with shared features of echinocandins lead to cross-resistance

The extent to which a mutation confers cross-resistance depends on the mutation mechanism of action, which can be explained with a model of drug binding. To better understand the molecular mechanisms underlying resistance, the mutants classified as either resistant or sensitive were grouped based on the type of amino acid substitution, i.e. the change in electrostatic or size properties of the alternative residue (relative to the WT residue) (fig. S8).

F639, S643 and P647 are the most crucial residues for pan-echinocandin resistance, as shown in our DMS (Figs. 2B-D) and in accordance with a body of evidence from lab, lab-evolved and clinical strains of fungal organisms. Indeed, mutants at this position constitute most of the hotspots for which our machine-learning model accurately predicts resistance (Fig. 3B, S1 Data). Our binding model reveals P647 has the potential of altering the shape of the hotspot cavity,

therefore inhibiting drug binding while sparing protein function. The high electron density of F639 seems to favor drug binding and action. Indeed, mutation to a negatively charged residue is tolerated by anidulafungin (Fig. 5A and fig. S8). S643 forms hydrogen bonds with the core hydroxyl and amine groups of the drugs, possibly stabilizing the common binding conformation (Fig. 5A). This explains why 16 substitutions at this position confer pan-echinocandin resistance (Figs. 2J-L and fig. S8A).

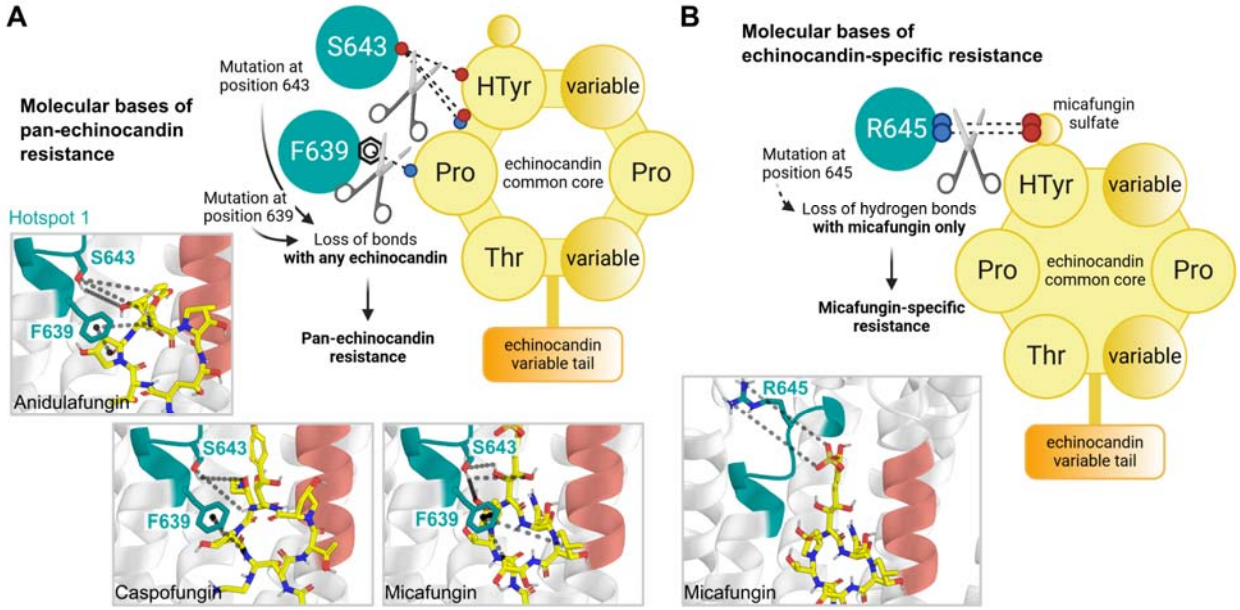

Fig. 5. Molecular bases of echinocandin resistance. (**A**) Example of pan-echinocandin resistance caused by the substitution of F639 or S643 in hotspot 1. A schematic representation of the drug structure shows features shared by all three echinocandins, including hydroxyls and amines belonging to the cyclic hexapeptide core (shown as single spheres for clarity; red or blue when including an oxygen or a nitrogen atom, respectively). Mutation of S643 can lead to the disruption of hydrogen bonds with these chemical groups, destabilizing drug binding regardless of the nature of the echinocandin, ultimately resulting in pan-echinocandin resistance. Similarly, loss of Van der Waals interactions between F639 and the proline residue from the core, or - dipole interactions with peptide bonds in the core, lead to cross-resistance. (**B**) Example of micafungin-specific resistance caused by the substitution of R645 in hotspot 1. The sulfate group specific to micafungin is highlighted. Mutation of R645 can lead to the disruption of hydrogen bonds between the guanidine group of the arginine and micafungin's sulfate. All four insets show the described bonds as dashed lines on the binding model, with the same color scheme as in Fig. 4. Schematic representations and figure insets were generated with BioRender and PyMol v2.5.5 (*28*), respectively.

We identified R645 in hotspot 1 as being key to micafungin-specific resistance, specifically when mutated to a negatively charged or aromatic residue (Fig. 2D and fig. S8). This suggests that micafungin is sensitive to high electron density functions at the extracellular part of the hotspot cavity. The docking poses corroborate this data, placing micafungin's sulfate function near R645 and the corresponding hydrogen bond acceptor FragMap (Fig. 2D and Fig. 5B). On the other hand, D646 is associated with resistance to anidulafungin and caspofungin, but not micafungin (Figs. 2B-D, fig. S8A). One of the five mutants illustrating this pattern is D646E, which demonstrates micafungin's tolerance to steric hindrance on the extracellular part of the

hotspot cavity. Indeed, near D646, a large generic hydrogen bond donor FragMap coincides with the drugs' weak hydrogen bond donor functions, mostly hydroxyls.

In hotspot 2, the echinocandin-specific resistance phenotypes of W1354 substitutions reveal anidulafungin can bind deep in the cavity (see supplementary text section S4, fig. S12). Also in hotspot 2, R1356 and R1357 mutations confer resistance to all three drugs. These arginines are located at the solvent-membrane interface, suggesting a role in phospholipid binding and potentially in membrane deformation. An observation supporting this structural role of positively charged residues in membrane deformation is the deleterious effect in the absence of drug of negatively charged aspartate or glutamate across hotspot 2 (Fig. 2E). Y1358 mutations conferring micafungin resistance also cause resistance to caspofungin (see supplementary text section S5). Together, these results provide explanations for why none of the hotspot 2 mutants sequenced in our DMS are resistant to micafungin only (fig. S5B). Instead, we do observe several hotspot 2 mutants being pan-echinocandin resistant or resistant to anidulafungin only (fig. S5B).

Beyond helping with the interpretation of the impact of mutations, our results show that echinocandins differ in their binding strength, which may help interpret their differences in efficacy. Caspofungin's weaker binding is attributed to superficial binding and steric hindrance from its large basic functions and a flexible hydrophobic tail. Consequently, caspofungin is more easily internalized in vacuoles, in which it is degraded by hydrolysis, ultimately diminishing drug efficacy (*22*). In contrast, anidulafungin resides on the fungal cell surface and does not get internalized (*22*). Instead, docking places it deep in the hotspot cavity in π-stacking proximity with the glucan translocation channel, which highlights the relationship between strong binding and inhibition of the target protein.

Interpreting the impact of mutations on potential treatment outcomes or improving drugs to overcome resistance mutations requires a solid knowledge of resistance mutations and a molecular model of drug binding. Predictions of the echinocandin susceptibility profile from sequence alone could help prescribe the most relevant echinocandin, increasing the chances of treatment success while helping to slow down the development of resistance. This approach has successfully been applied to the etiologic agents of malaria or tuberculosis (*23*, *24*), but has yet to be implemented in fungi. Our data and recent work on other antifungal drug targets (*25*, *26*) contribute to this collective effort.

Beyond improving drug stewardship, elucidating the molecular mechanisms of echinocandin resistance and binding specificity has highlighted key elements in the structures of both the drugs and their target, which provide valuable information for the rational modification of existing drugs and design of novel compounds targeting Fks1. For instance, our results have highlighted residues outside of the hotspots that are important for drug binding. The reason they were not as frequently reported as being associated with resistance might lie in diagnostics biases (for example sequencing only the "traditional" hotspots). Alternatively, these residues could be less mutationally tolerant than the ones in hotspot 1, for example because they play an important role in the enzyme's structure or function. This information could be leveraged to re-design existing echinocandins by stabilizing interactions with these mutationally fragile residues. As a result, resistance would emerge much more slowly because it would come with a strong fitness cost.

References and Notes

1. P. G. Pappas, C. A. Kauffman, D. R. Andes, C. J. Clancy, K. A. Marr, L. Ostrosky-Zeichner, A. C. Reboli, M. G. Schuster, J. A. Vazquez, T. J. Walsh, T. E. Zaoutis, J. D. Sobel, Clinical Practice Guideline for the Management of Candidiasis: 2016 Update by the Infectious Diseases Society of America. *Clin. Infect. Dis.* **62**, e1–50 (2016).

2. A. Chowdhary, C. Sharma, J. F. Meis, Candida auris: A rapidly emerging cause of hospital-acquired multidrug-resistant fungal infections globally. *PLoS Pathog.* **13**, e1006290 (2017).

3. Y. Lee, N. Robbins, L. E. Cowen, Molecular mechanisms governing antifungal drug resistance. *npj Antimicrobials and Resistance* **1**, 1–9 (2023).

4. L. A. Walker, N. A. R. Gow, C. A. Munro, Fungal echinocandin resistance. *Fungal Genet. Biol.* **47**, 117–126 (2010).

5. M. A. Pfaller, D. J. Diekema, J. D. Turnidge, M. Castanheira, R. N. Jones, Twenty years of the SENTRY antifungal surveillance program: Results for Candida species from 1997-2016. *Open Forum Infect. Dis.* **6**, S79–S94 (2019).

6. G. Garcia-Effron, Rezafungin-Mechanisms of Action, Susceptibility and Resistance: Similarities and Differences with the Other Echinocandins. *J Fungi (Basel)* **6** (2020).

7. X. Hu, P. Yang, C. Chai, J. Liu, H. Sun, Y. Wu, M. Zhang, M. Zhang, X. Liu, H. Yu, Structural and mechanistic insights into fungal β-1,3-glucan synthase FKS1. *Nature*, doi: 10.1038/s41586-023-05856-5 (2023).

8. M. Jospe-Kaufman, E. Ben-Zeev, A. Mottola, A. Dukhovny, J. Berman, S. Carmeli, M. Fridman, Reshaping echinocandin antifungal drugs to circumvent glucan synthase point□mutation□mediated resistance. *Angew. Chem. Weinheim Bergstr. Ger.*, doi: 10.1002/ange.202314728 (2024).

9. C. E. Faller, E. P. Raman, A. D. MacKerell Jr, O. Guvench, Site Identification by Ligand Competitive Saturation (SILCS) simulations for fragment-based drug design. *Methods Mol. Biol.* **1289**, 75–87 (2015).

10. P. Mazur, N. Morin, W. Baginsky, M. el-Sherbeini, J. A. Clemas, J. B. Nielsen, F. Foor, Differential expression and function of two homologous subunits of yeast 1,3-beta-D-glucan synthase. *Mol. Cell. Biol.* **15**, 5671–5681 (1995).

11. E. Puumala, S. Fallah, N. Robbins, L. E. Cowen, Advancements and challenges in antifungal therapeutic development. *Clin. Microbiol. Rev.* **37**, e0014223 (2024).

12. B. D. Alexander, M. D. Johnson, C. D. Pfeiffer, C. Jiménez-Ortigosa, J. Catania, R. Booker, M. Castanheira, S. A. Messer, D. S. Perlin, M. A. Pfaller, Increasing echinocandin resistance in Candida glabrata: clinical failure correlates with presence of FKS mutations and elevated minimum inhibitory concentrations. *Clin. Infect. Dis.* **56**, 1724–1732 (2013).

13. C. D. Pham, N. Iqbal, C. B. Bolden, R. J. Kuykendall, L. H. Harrison, M. M. Farley, W. Schaffner, Z. G. Beldavs, T. M. Chiller, B. J. Park, A. A. Cleveland, S. R. Lockhart, Role of FKS Mutations in Candida glabrata: MIC values, echinocandin resistance, and multidrug resistance. *Antimicrob. Agents Chemother.* **58**, 4690–4696 (2014).

14. Garcia-Effron Guillermo, Lee Samuel, Park Steven, Cleary John D., Perlin David S., Effect of Candida glabrata FKS1 and FKS2 Mutations on Echinocandin Sensitivity and Kinetics of 1,3-β-d-Glucan Synthase: Implication for the Existing Susceptibility Breakpoint. *Antimicrob. Agents Chemother.* **53**, 3690–3699 (2009).

15. WHO fungal priority pathogens list to guide research, development and public health action (2022). https://www.who.int/publications/i/item/9789240060241.

16. G. Garcia-Effron, S. K. Katiyar, S. Park, T. D. Edlind, D. S. Perlin, A naturally occurring proline-to-alanine amino acid change in Fks1p in Candida parapsilosis, Candida orthopsilosis, and Candida metapsilosis accounts for reduced echinocandin susceptibility. *Antimicrob. Agents Chemother.* **52**, 2305–2312 (2008).

17. G. K. Abruzzo, A. M. Flattery, C. J. Gill, L. Kong, J. G. Smith, V. B. Pikounis, J. M. Balkovec, A. F. Bouffard, J. F. Dropinski, H. Rosen, H. Kropp, K. Bartizal, Evaluation of the echinocandin antifungal MK-0991 (L-743,872): efficacies in mouse models of disseminated aspergillosis, candidiasis, and cryptococcosis. *Antimicrob. Agents Chemother.* **41**, 2333–2338 (1997).

18. M. Lackner, M. Tscherner, M. Schaller, K. Kuchler, C. Mair, B. Sartori, F. Istel, M. C. Arendrup, C. Lass-Flörl, Positions and numbers of FKS mutations in Candida albicans selectively influence in vitro and in vivo susceptibilities to echinocandin treatment. *Antimicrob. Agents Chemother.* **58**, 3626–3635 (2014).

19. R. Ben-Ami, G. Garcia-Effron, R. E. Lewis, S. Gamarra, K. Leventakos, D. S. Perlin, D. P. Kontoyiannis, Fitness and virulence costs of Candida albicans FKS1 hot spot mutations associated with echinocandin resistance. *J. Infect. Dis.* **204**, 626–635 (2011).

20. M. Szymański, S. Chmielewska, U. Czyżewska, M. Malinowska, A. Tylicki, Echinocandins - structure, mechanism of action and use in antifungal therapy. *J. Enzyme Inhib. Med. Chem.* **37**, 876–894 (2022).

21. E. Spreghini, F. Orlando, M. Sanguinetti, B. Posteraro, D. Giannini, E. Manso, F. Barchiesi, Comparative effects of micafungin, caspofungin, and anidulafungin against a difficult-to-treat fungal opportunistic pathogen, Candida glabrata. *Antimicrob. Agents Chemother.* **56**, 1215–1222 (2012).

22. Q. Z. Jaber, D. Logviniuk, A. Yona, M. Fridman, Echinocandins localized to the target-harboring cell surface are not degraded but those entering the vacuole are. *ACS Chem. Biol.* **17**, 1155–1163 (2022).

23. S. G. Murphy, C. Smith, P. Lapierre, J. Shea, K. Patel, T. A. Halse, M. Dickinson, V. Escuyer, M. C. Rowlinson, K. A. Musser, Direct detection of drug-resistant Mycobacterium tuberculosis using targeted next generation sequencing. *Front. Public Health* **11**, 1206056 (2023).

24. G. Pines, R. G. Fankhauser, C. A. Eckert, Predicting Drug Resistance Using Deep Mutational Scanning. *Molecules* **25** (2020).

25. C. Bédard, I. Gagnon-Arsenault, J. Boisvert, S. Plante, A. K. Dubé, A. Pageau, J. Sharma, L. Maroc, R. S. Shapiro, C. R. Landry, Most azole antifungal resistance mutations in the drug target provide cross-resistance and carry no intrinsic fitness cost, *bioRxiv* (2023)p. 2023.12.13.571438.

26. P. C. Després, A. F. Cisneros, E. M. M. Alexander, R. Sonigara, C. Gagné-Thivierge, A. K. Dubé, C. R. Landry, Asymmetrical dose responses shape the evolutionary trade-off between antifungal resistance and nutrient use. *Nat Ecol Evol* **6**, 1501–1515 (2022).

27. E. F. Pettersen, T. D. Goddard, C. C. Huang, E. C. Meng, G. S. Couch, T. I. Croll, J. H. Morris, T. E. Ferrin, UCSF ChimeraX: Structure visualization for researchers, educators, and developers. *Protein Sci.* **30**, 70–82 (2021).

28. Schrödinger, LLC, The PyMOL Molecular Graphics System, Version 2.5.5. [Preprint] (2015).

29. M. Lõoke, K. Kristjuhan, A. Kristjuhan, Extraction of genomic DNA from yeasts for PCR-based applications. *Biotechniques* **50**, 325–328 (2011).

30. S. Mnaimneh, A. P. Davierwala, J. Haynes, J. Moffat, W.-T. Peng, W. Zhang, X. Yang, J. Pootoolal, G. Chua, A. Lopez, M. Trochesset, D. Morse, N. J. Krogan, S. L. Hiley, Z. Li, Q. Morris, J. Grigull, N. Mitsakakis, C. J. Roberts, J. F. Greenblatt, C. Boone, C. A. Kaiser, B. J. Andrews, T. R. Hughes, Exploration of essential gene functions via titratable promoter alleles. *Cell* **118**, 31–44 (2004).

31. O. W. Ryan, S. Poddar, J. H. D. Cate, CRISPR-Cas9 Genome Engineering in Saccharomyces cerevisiae Cells. *Cold Spring Harb. Protoc.* **2016** (2016).

32. L. P. Pryszcz, J. Huerta-Cepas, T. Gabaldón, MetaPhOrs: orthology and paralogy predictions from multiple phylogenetic evidence using a consistency-based confidence score. *Nucleic Acids Res.* **39**, e32 (2011).

33. R. C. Edgar, MUSCLE: multiple sequence alignment with high accuracy and high throughput. *Nucleic Acids Res.* **32**, 1792–1797 (2004).

34. S. Capella-Gutiérrez, J. M. Silla-Martínez, T. Gabaldón, trimAl: a tool for automated alignment trimming in large-scale phylogenetic analyses. *Bioinformatics* **25**, 1972–1973 (2009).

35. D. C. Amberg, D. J. Burke, J. N. Strathern, "Yeast DNA Isolations, Techniques and Protocols 3" in *Methods in Yeast Genetics* (Cold Spring Harbor Laboratory Press, 2005).

36. N. Yachie, E. Petsalaki, J. C. Mellor, J. Weile, Y. Jacob, M. Verby, S. B. Ozturk, S. Li, A. G. Cote, R. Mosca, J. J. Knapp, M. Ko, A. Yu, M. Gebbia, N. Sahni, S. Yi, T. Tyagi, D. Sheykhkarimli, J. F. Roth, C. Wong, L. Musa, J. Snider, Y.-C. Liu, H. Yu, P. Braun, I. Stagljar, T. Hao, M. A. Calderwood, L. Pelletier, P. Aloy, D. E. Hill, M. Vidal, F. P. Roth, Pooled-matrix protein interaction screens using Barcode Fusion Genetics. *Mol. Syst. Biol.* **12**, 863 (2016).

37. J. M. Cota, J. L. Grabinski, R. L. Talbert, D. S. Burgess, P. D. Rogers, T. D. Edlind, N. P. Wiederhold, Increases in SLT2 expression and chitin content are associated with incomplete killing of Candida glabrata by caspofungin. *Antimicrob. Agents Chemother.* **52**, 1144–1146 (2008).

38. A. J. Faure, J. M. Schmiedel, P. Baeza-Centurion, B. Lehner, DiMSum: an error model and pipeline for analyzing deep mutational scanning data and diagnosing common experimental pathologies. *Genome Biol.* **21**, 207 (2020).

39. E. Gasteiger, C. Hoogland, A. Gattiker, S. 'everine Duvaud, M. R. Wilkins, R. D. Appel, A. Bairoch, "Protein Identification and Analysis Tools on the ExPASy Server" in *The Proteomics Protocols Handbook*, J. M. Walker, Ed. (Humana Press, Totowa, NJ, 2005), pp. 571–607.

40. E. D. Levy, S. De, S. A. Teichmann, Cellular crowding imposes global constraints on the chemistry and evolution of proteomes. *Proc. Natl. Acad. Sci. U. S. A.* **109**, 20461–20466 (2012).

41. E. A. Coutsias, C. Seok, M. P. Jacobson, K. A. Dill, A kinematic view of loop closure. *J. Comput. Chem.* **25**, 510–528 (2004).

42. S. Jo, T. Kim, V. G. Iyer, W. Im, CHARMM-GUI: a web-based graphical user interface for CHARMM. *J. Comput. Chem.* **29**, 1859–1865 (2008).

43. 2022. 02 Chemical Computing Group ULC, Molecular Operating Environment (MOE). [Preprint] (2024).

44. E. Jurrus, D. Engel, K. Star, K. Monson, J. Brandi, L. E. Felberg, D. H. Brookes, L. Wilson, J. Chen, K. Liles, M. Chun, P. Li, D. W. Gohara, T. Dolinsky, R. Konecny, D. R. Koes, J. E. Nielsen, T. Head-Gordon, W. Geng, R. Krasny, G.-W. Wei, M. J. Holst, J. A. McCammon, N. A. Baker, Improvements to the APBS biomolecular solvation software suite. *Protein Sci.* **27**, 112–128 (2018).

45. A. L. Lomize, S. C. Todd, I. D. Pogozheva, Spatial arrangement of proteins in planar and curved membranes by PPM 3.0. *Protein Sci.* **31**, 209–220 (2022).

46. E. L. Wu, X. Cheng, S. Jo, H. Rui, K. C. Song, E. M. Dávila-Contreras, Y. Qi, J. Lee, V. Monje-Galvan, R. M. Venable, J. B. Klauda, W. Im, CHARMM-GUI Membrane Builder toward realistic biological membrane simulations. *J. Comput. Chem.* **35**, 1997–2004 (2014).

47. I. D. Pogozheva, G. A. Armstrong, L. Kong, T. J. Hartnagel, C. A. Carpino, S. E. Gee, D. M. Picarello, A. S. Rubin, J. Lee, S. Park, A. L. Lomize, W. Im, Comparative Molecular Dynamics Simulation Studies of Realistic Eukaryotic, Prokaryotic, and Archaeal Membranes. *J. Chem. Inf. Model.* **62**, 1036–1051 (2022).

48. J. C. Phillips, D. J. Hardy, J. D. C. Maia, J. E. Stone, J. V. Ribeiro, R. C. Bernardi, R. Buch, G. Fiorin, J. Hénin, W. Jiang, R. McGreevy, M. C. R. Melo, B. K. Radak, R. D. Skeel, A. Singharoy, Y. Wang, B. Roux, A. Aksimentiev, Z. Luthey-Schulten, L. V. Kalé, K. Schulten, C. Chipot, E. Tajkhorshid, Scalable molecular dynamics on CPU and GPU architectures with NAMD. *J. Chem. Phys.* **153**, 044130 (2020).

49. J. Huang, S. Rauscher, G. Nawrocki, T. Ran, M. Feig, B. L. de Groot, H. Grubmüller, A. D. MacKerell Jr, CHARMM36m: an improved force field for folded and intrinsically disordered proteins. *Nat. Methods* **14**, 71–73 (2017).

50. S. R. Durell, B. R. Brooks, A. Ben-Naim, Solvent-Induced Forces between Two Hydrophilic Groups. *J. Phys. Chem.* **98**, 2198–2202 (1994).

51. Y. Gao, J. Lee, I. P. S. Smith, H. Lee, S. Kim, Y. Qi, J. B. Klauda, G. Widmalm, S. Khalid, W. Im, CHARMM-GUI Supports Hydrogen Mass Repartitioning and Different Protonation States of Phosphates in Lipopolysaccharides. *J. Chem. Inf. Model.* **61**, 831–839 (2021).

52. S. Miyamoto, P. A. Kollman, Settle: An analytical version of the SHAKE and RATTLE algorithm for rigid water models. *J. Comput. Chem.* **13**, 952–962 (1992).

53. J.-P. Ryckaert, G. Ciccotti, H. J. C. Berendsen, Numerical integration of the cartesian equations of motion of a system with constraints: molecular dynamics of n-alkanes. *J. Comput. Phys.* **23**, 327–341 (1977).

54. T. Darden, D. York, L. Pedersen, Particle mesh Ewald: An N·log(N) method for Ewald sums in large systems. *J. Chem. Phys.* **98**, 10089–10092 (1993).

55. A. D. MacKerell Jr, S. Jo, S. K. Lakkaraju, C. Lind, W. Yu, Identification and characterization of fragment binding sites for allosteric ligand design using the site identification by ligand competitive saturation hotspots approach (SILCS-Hotspots). *Biochim. Biophys. Acta Gen. Subj*. **1864**, 129519 (2020).

56. S. Kumar, G. Stecher, M. Li, C. Knyaz, K. Tamura, MEGA X: Molecular Evolutionary Genetics Analysis across Computing Platforms. *Mol. Biol. Evol.* **35**, 1547–1549 (2018).

57. S. Q. Le, O. Gascuel, An Improved General Amino Acid Replacement Matrix. *Mol. Biol. Evol.* **25**, 1307–1320 (2008).

58. J. D. Hunter, Matplotlib: A 2D Graphics Environment. *Comput. Sci. Eng.* **9**, 90–95 (2007).

59. C. R. Harris, K. J. Millman, S. J. van der Walt, R. Gommers, P. Virtanen, D. Cournapeau, E. Wieser, J. Taylor, S. Berg, N. J. Smith, R. Kern, M. Picus, S. Hoyer, M. H. van Kerkwijk, M. Brett, A. Haldane, J. F. Del Río, M. Wiebe, P. Peterson, P. Gérard-Marchant, K. Sheppard, T. Reddy, W. Weckesser, H. Abbasi, C. Gohlke, T. E. Oliphant, Array programming with NumPy. *Nature* **585**, 357–362 (2020).

60. W. McKinney, "Data Structures for Statistical Computing in Python" in *PRoceedings of the 9th PYthon in SCience COnference*, S. van der Walt, J. Millman, Eds. (SciPy, 2010; http://dx.doi.org/10.25080/Majora-92bf1922-00a).

61. F. Pedregosa, G. Varoquaux, A. Gramfort, V. Michel, B. Thirion, O. Grisel, M. Blondel, G. Louppe, P. Prettenhofer, R. Weiss, R. J. Weiss, J. Vanderplas, A. Passos, D. Cournapeau, M. Brucher, M. Perrot, E. Duchesnay, Scikit-learn: Machine Learning in Python. *J. Mach. Learn. Res.* **abs/1201.0490** (2011).

62. P. Virtanen, R. Gommers, T. E. Oliphant, M. Haberland, T. Reddy, D. Cournapeau, E. Burovski, P. Peterson, W. Weckesser, J. Bright, S. J. van der Walt, M. Brett, J. Wilson, K. J. Millman, N. Mayorov, A. R. J. Nelson, E. Jones, R. Kern, E. Larson, C. J. Carey, İ. Polat, Y. Feng, E. W. Moore, J. VanderPlas, D. Laxalde, J. Perktold, R. Cimrman, I. Henriksen, E. A. Quintero, C. R. Harris, A. M. Archibald, A. H. Ribeiro, F. Pedregosa, P. van Mulbregt, SciPy 1.0 Contributors, SciPy 1.0: fundamental algorithms for scientific computing in Python. *Nat. Methods* **17**, 261–272 (2020).

63. M. Waskom, seaborn: statistical data visualization. *J. Open Source Softw.* **6**, 3021 (2021).

64. S. M. Lundberg, S.-I. Lee, "A Unified Approach to Interpreting Model Predictions" in *Advances in Neural Information Processing Systems 30*, I. Guyon, U. V. Luxburg, S. Bengio, H. Wallach, R. Fergus, S. Vishwanathan, R. Garnett, Eds. (Curran Associates, Inc., 2017), pp. 4765–4774.

65. C.-R. Zhao, Z.-L. You, D.-D. Chen, J. Hang, Z.-B. Wang, M. Ji, L.-X. Wang, P. Zhao, J. Qiao, C.-H. Yun, L. Bai, Structure of a fungal 1,3-β-glucan synthase. *Sci. Adv.* **9**, eadh7820 (2023).

66. R. Cowan, R. G. Whittaker, Hydrophobicity indices for amino acid residues as determined by high-performance liquid chromatography. *Pept. Res.* **3**, 75–80 (1990).

67. M. Levitt, Conformational preferences of amino acids in globular proteins. *Biochemistry* **17**, 4277–4285 (1978).

68. S. Lifson, C. Sander, Antiparallel and parallel beta-strands differ in amino acid residue preferences. *Nature* **282**, 109–111 (1979).

69. C. Tanford, Contribution of hydrophobic interactions to the stability of the globular conformation of proteins. *J. Am. Chem. Soc.* **84**, 4240–4247 (1962).

70. G. W. Welling, W. J. Weijer, R. van der Zee, S. Welling-Wester, Prediction of sequential antigenic regions in proteins. *FEBS Lett.* **188**, 215–218 (1985).

71. S. D. Black, D. R. Mould, Development of hydrophobicity parameters to analyze proteins which bear post- or cotranslational modifications. *Anal. Biochem.* **193**, 72–82 (1991).

72. M. Dayhoff, R. Schwartz, B. Orcutt, 22. A model of evolutionary change in proteins. *Atlas of protein sequence and structure* **5**, 345–352 (1978).

73. R. Bhaskaran, P. K. Ponnuswamy, Positional flexibilities of amino acid residues in globular proteins. *Int. J. Pept. Protein Res.* **32**, 241–255 (1988).

74. S. Miyazawa, R. L. Jernigan, Estimation of effective interresidue contact energies from protein crystal structures: quasi-chemical approximation. *Macromolecules* **18**, 534–552 (1985).

75. J. M. Parker, D. Guo, R. S. Hodges, New hydrophilicity scale derived from high-performance liquid chromatography peptide retention data: correlation of predicted surface residues with antigenicity and X-ray-derived accessible sites. *Biochemistry* **25**, 5425–5432 (1986).

76. J. Fauchere, V. Pliska, Hydrophobic parameters II of amino acid side-chains from the partitioning of N-acetyl-amino acid amides. *Eur. J. Med. Chem.* **18** (01 1983).

77. A. F. Cisneros, I. Gagnon-Arsenault, A. K. Dubé, P. C. Després, P. Kumar, K. Lafontaine, J. N. Pelletier, C. R. Landry, Epistasis between promoter activity and coding mutations shapes gene evolvability. *Sci Adv* **9**, eadd9109 (2023).

78. R. E. Gardiner, P. Souteropoulos, S. Park, D. S. Perlin, Characterization of Aspergillus fumigatus mutants with reduced susceptibility to caspofungin. *Med. Mycol.* **43 Suppl 1**, S299–305 (2005).

79. O. Avramovska, A. C. Smith, E. Rego, M. A. Hickman, Tetraploidy accelerates adaptation under drug selection in a fungal pathogen. *Front. Fungal Biol.* **3**, 984377 (2022).

80. G. Garcia-Effron, S. Park, D. S. Perlin, Correlating echinocandin MIC and kinetic inhibition of fks1 mutant glucan synthases for Candida albicans: implications for interpretive breakpoints. *Antimicrob. Agents Chemother.* **53**, 112–122 (2009).

81. S. V. Balashov, S. Park, D. S. Perlin, Assessing resistance to the echinocandin antifungal drug caspofungin in Candida albicans by profiling mutations in FKS1. *Antimicrob. Agents Chemother.* **50**, 2058–2063 (2006).

82. S. Park, R. Kelly, J. N. Kahn, J. Robles, M.-J. Hsu, E. Register, W. Li, V. Vyas, H. Fan, G. Abruzzo, A. Flattery, C. Gill, G. Chrebet, S. A. Parent, M. Kurtz, H. Teppler, C. M. Douglas, D. S. Perlin, Specific substitutions in the echinocandin target Fks1p account for reduced susceptibility of rare laboratory and clinical Candida sp. isolates. *Antimicrob. Agents Chemother.* **49**, 3264–3273 (2005).

83. G. Garcia-Effron, D. J. Chua, J. R. Tomada, J. DiPersio, D. S. Perlin, M. Ghannoum, H. Bonilla, Novel FKS mutations associated with echinocandin resistance in Candida species. *Antimicrob. Agents Chemother.* **54**, 2225–2227 (2010).

84. M. Castanheira, L. M. Deshpande, A. P. Davis, P. R. Rhomberg, M. A. Pfaller, Monitoring Antifungal Resistance in a Global Collection of Invasive Yeasts and Molds: Application of CLSI Epidemiological Cutoff Values and Whole-Genome Sequencing Analysis for Detection of Azole Resistance in Candida albicans. *Antimicrob. Agents Chemother.* **61** (2017).

85. M. Castanheira, L. M. Deshpande, S. A. Messer, P. R. Rhomberg, M. A. Pfaller, Analysis of global antifungal surveillance results reveals predominance of Erg11 Y132F alteration among azole-resistant Candida parapsilosis and Candida tropicalis and country-specific isolate dissemination. *Int. J. Antimicrob. Agents* **55**, 105799 (2020).

86. C. D. Miller, B. W. Lomaestro, S. Park, D. S. Perlin, Progressive esophagitis caused by Candida albicans with reduced susceptibility to caspofungin. *Pharmacotherapy* **26**, 877–880 (2006).

87. M. Desnos-Ollivier, S. Bretagne, D. Raoux, D. Hoinard, F. Dromer, E. Dannaoui, European Committee on Antibiotic Susceptibility Testing, Mutations in the fks1 gene in Candida albicans, C. tropicalis, and C. krusei correlate with elevated caspofungin MICs uncovered in AM3 medium using the method of the European Committee on Antibiotic Susceptibility Testing. *Antimicrob. Agents Chemother.* **52**, 3092–3098 (2008).

88. Y. Zhu, K. M. Hager, S. R. Manjari, N. K. Banavali, V. Chaturvedi, S. Chaturvedi, Development and Validation of TaqMan Chemistry Probe-Based Rapid Assay for the Detection of Echinocandin-Resistance in Candida auris. *J. Clin. Microbiol.* **61**, e0176722 (2023).

89. A. Chowdhary, A. Prakash, C. Sharma, M. Kordalewska, A. Kumar, S. Sarma, B. Tarai, A. Singh, G. Upadhyaya, S. Upadhyay, P. Yadav, P. K. Singh, V. Khillan, N. Sachdeva, D. S. Perlin, J. F. Meis, A multicentre study of antifungal susceptibility patterns among 350 Candida auris isolates (2009-17) in India: role of the ERG11 and FKS1 genes in azole and echinocandin resistance. *J. Antimicrob. Chemother.* **73**, 891–899 (2018).

90. M. Kordalewska, A. Lee, S. Park, I. Berrio, A. Chowdhary, Y. Zhao, D. S. Perlin, Understanding Echinocandin Resistance in the Emerging Pathogen Candida auris. *Antimicrob. Agents Chemother.* **62** (2018).

91. K. L. Chew, S. Octavia, R. Jureen, R. T. P. Lin, J. W. P. Teo, Targeted amplification and MinION nanopore sequencing of key azole and echinocandin resistance determinants of clinically relevant Candida spp. from blood culture bottles. *Lett. Appl. Microbiol.* **73**, 286–293 (2021).

92. T. Hirayama, T. Miyazaki, M. Sumiyoshi, Y. Ito, N. Ashizawa, K. Takeda, N. Iwanaga, T. Takazono, K. Yamamoto, K. Izumikawa, K. Yanagihara, K. Makimura, K. Tsukamoto, S. Kohno, H. Mukae, Echinocandin Resistance in Candida auris Occurs in the Murine Gastrointestinal Tract Due to FKS1 Mutations. *Antimicrob. Agents Chemother.* **67**, e0124322 (2023).

93. E. L. Berkow, S. R. Lockhart, Activity of CD101, a long-acting echinocandin, against clinical isolates of Candida auris. *Diagn. Microbiol. Infect. Dis.* **90**, 196–197 (2018).

94. M. J. Biagi, N. P. Wiederhold, C. Gibas, B. L. Wickes, V. Lozano, S. C. Bleasdale, L. Danziger, Development of High-Level Echinocandin Resistance in a Patient With Recurrent Candida auris Candidemia Secondary to Chronic Candiduria. *Open Forum Infect Dis* **6**, ofz262 (2019).

95. J. F. Staab, D. Neofytos, P. Rhee, C. Jiménez-Ortigosa, S. X. Zhang, D. S. Perlin, K. A. Marr, Target enzyme mutations confer differential echinocandin susceptibilities in Candida kefyr. *Antimicrob. Agents Chemother.* **58**, 5421–5427 (2014).

96. J. N. Kahn, G. Garcia-Effron, M.-J. Hsu, S. Park, K. A. Marr, D. S. Perlin, Acquired echinocandin resistance in a Candida krusei isolate due to modification of glucan synthase. *Antimicrob. Agents Chemother.* **51**, 1876–1878 (2007).

97. I. Accoceberry, C. Couzigou, V. Fitton-Ouhabi, N. Biteau, T. Noël, Challenging SNP impact on caspofungin resistance by full-length FKS1 allele replacement in Candida lusitaniae. *J. Antimicrob. Chemother.* **74**, 618–624 (2019).

98. Y. Ning, M. Xiao, D. S. Perlin, Y. Zhao, M. Lu, Y. Li, Z. Luo, R. Dai, S. Li, J. Xu, L. Liu, H. He, Y. Liu, F. Li, Y. Guo, Z. Chen, Y. Xu, T. Sun, L. Zhang, Decreased echinocandin susceptibility in Candida parapsilosis causing candidemia and emergence of a pan-echinocandin resistant case in China. *Emerg. Microbes Infect.* **12**, 2153086 (2023).

99. C. Keighley, M. Gall, S. J. van Hal, C. L. Halliday, L. Y. A. Chai, K. L. Chew, C. Biswas, M. A. Slavin, W. Meyer, V. Sintchenko, S. C. A. Chen, Whole Genome Sequencing Shows Genetic Diversity, as Well as Clonal Complex and Gene Polymorphisms Associated with Fluconazole Non-Susceptible Isolates of Candida tropicalis. *J Fungi (Basel)* **8** (2022).

100. E. Ksiezopolska, M. À. Schikora-Tamarit, R. Beyer, J. C. Nunez-Rodriguez, C. Schüller, T. Gabaldón, Narrow mutational signatures drive acquisition of multidrug resistance in the fungal pathogen Candida glabrata. *Curr. Biol.* **0** (2021).

101. C. Dudiuk, S. Gamarra, F. Leonardeli, C. Jimenez-Ortigosa, R. G. Vitale, J. Afeltra, D. S. Perlin, G. Garcia-Effron, Set of classical PCRs for detection of mutations in Candida glabrata FKS genes linked with echinocandin resistance. *J. Clin. Microbiol.* **52**, 2609–2614 (2014).

102. G. Garcia-Effron, S. Lee, S. Park, J. D. Cleary, D. S. Perlin, Effect of Candida glabrata FKS1 and FKS2 mutations on echinocandin sensitivity and kinetics of 1,3-beta-D-glucan synthase: implication for the existing susceptibility breakpoint. *Antimicrob. Agents Chemother.* **53**, 3690–3699 (2009).

103. A. J. Zimbeck, N. Iqbal, A. M. Ahlquist, M. M. Farley, L. H. Harrison, T. Chiller, S. R. Lockhart, FKS mutations and elevated echinocandin MIC values among Candida glabrata isolates from U.S. population-based surveillance. *Antimicrob. Agents Chemother.* **54**, 5042–5047 (2010).

104. M. C. Arendrup, D. S. Perlin, R. H. Jensen, S. J. Howard, J. Goodwin, W. Hope, Differential in vivo activities of anidulafungin, caspofungin, and micafungin against Candida glabrata isolates with and without FKS resistance mutations. *Antimicrob. Agents Chemother.* **56**, 2435–2442 (2012).

105. A. Lepak, M. Castanheira, D. Diekema, M. Pfaller, D. Andes, Optimizing Echinocandin dosing and susceptibility breakpoint determination via in vivo pharmacodynamic evaluation against Candida glabrata with and without fks mutations. *Antimicrob. Agents Chemother.* **56**, 5875–5882 (2012).

106. M. Castanheira, L. N. Woosley, S. A. Messer, D. J. Diekema, R. N. Jones, M. A. Pfaller, Frequency of fks mutations among Candida glabrata isolates from a 10-year global collection of bloodstream infection isolates. *Antimicrob. Agents Chemother.* **58**, 577–580 (2014).

107. M. Fraser, A. M. Borman, R. Thorn, L. M. Lawrance, Resistance to echinocandin antifungal agents in the United Kingdom in clinical isolates of Candida glabrata: Fifteen years of interpretation and assessment. *Med. Mycol.* **58**, 219–226 (2020).

108. A. T. Coste, A. Kritikos, J. Li, N. Khanna, D. Goldenberger, C. Garzoni, C. Zehnder, K. Boggian, D. Neofytos, A. Riat, D. Bachmann, D. Sanglard, F. Lamoth, Fungal Infection Network of Switzerland (FUNGINOS), Emerging echinocandin-resistant Candida albicans and glabrata in Switzerland. *Infection* **48**, 761–766 (2020).

109. M. A. Pfaller, S. A. Messer, D. J. Diekema, R. N. Jones, M. Castanheira, Use of micafungin as a surrogate marker to predict susceptibility and resistance to caspofungin among 3,764 clinical isolates of Candida by use of CLSI methods and interpretive criteria. *J. Clin. Microbiol.* **52**, 108–114 (2014).

110. C. Biswas, V. R. Marcelino, S. Van Hal, C. Halliday, E. Martinez, Q. Wang, S. Kidd, K. Kennedy, D. Marriott, C. O. Morrissey, I. Arthur, K. Weeks, M. A. Slavin, T. C. Sorrell, V. Sintchenko, W. Meyer, S. C.-A. Chen, Whole Genome Sequencing of Australian Candida glabrata Isolates Reveals Genetic Diversity and Novel Sequence Types. *Front. Microbiol.* **9**, 2946 (2018).

111. J. D. Cleary, G. Garcia-Effron, S. W. Chapman, D. S. Perlin, Reduced Candida glabrata susceptibility secondary to an FKS1 mutation developed during candidemia treatment. *Antimicrob. Agents Chemother.* **52**, 2263–2265 (2008).

112. R. K. Shields, M. H. Nguyen, E. G. Press, A. L. Kwa, S. Cheng, C. Du, C. J. Clancy, The presence of an FKS mutation rather than MIC is an independent risk factor for failure of echinocandin therapy among patients with invasive candidiasis due to Candida glabrata. *Antimicrob. Agents Chemother.* **56**, 4862–4869 (2012).

113. S. Memon, N. K. Ghanchi, U. Zafar, J. Farooqi, S. Zaka, K. Jabeen, Analysis of fks1 and fks2 gene mutations in invasive Candida glabrata strains from Pakistan. *Mycoses* **66**, 52–58 (2023).

114. R. K. Shields, M. H. Nguyen, E. G. Press, R. Cumbie, E. Driscoll, A. W. Pasculle, C. J. Clancy, Rate of FKS Mutations among Consecutive Candida Isolates Causing Bloodstream Infection. *Antimicrob. Agents Chemother.* **59**, 7465–7470 (2015).

115. C. Garnaud, F. Botterel, N. Sertour, M.-E. Bougnoux, E. Dannaoui, S. Larrat, C. Hennequin, J. Guinea, M. Cornet, D. Maubon, Next-generation sequencing offers new insights into the resistance of Candida spp. to echinocandins and azoles. *J. Antimicrob. Chemother.* **70**, 2556–2565 (2015).

116. M. Á. Bordallo-Cardona, P. Escribano, E. G. G. de la Pedrosa, L. J. Marcos-Zambrano, R. Cantón, E. Bouza, J. Guinea, In vitro exposure to increasing micafungin concentrations easily promotes echinocandin resistance in Candida glabrata isolates. *Antimicrob. Agents Chemother.* **61**, AAC.01542–16 (2017).

117. M. Á. Bordallo-Cardona, P. Escribano, L. J. Marcos-Zambrano, J. Díaz-García, E. G. de la Pedrosa, R. Cantón, E. Bouza, J. Guinea, Low and constant micafungin concentrations may be

sufficient to lead to resistance mutations in FKS2 gene of Candida glabrata. *Med. Mycol.* **56**, 903–906 (2018).

118. K. Spettel, W. Barousch, A. Makristathis, I. Zeller, M. Nehr, B. Selitsch, M. Lackner, P.-M. Rath, J. Steinmann, B. Willinger, Analysis of antifungal resistance genes in Candida albicans and Candida glabrata using next generation sequencing. *PLoS One* **14**, e0210397 (2019).

119. O. Rivero-Menendez, P. Navarro-Rodriguez, L. Bernal-Martinez, G. Martin-Cano, L. Lopez-Perez, I. Sanchez-Romero, A. Perez-Ayala, J. Capilla, O. Zaragoza, A. Alastruey-Izquierdo, Clinical and laboratory development of echinocandin resistance in Candida glabrata: Molecular characterization. *Front. Microbiol.* **10**, 1585 (2019).

120. A. K. Sig, M. C. Sonmezer, D. Gülmez, S. Duyan, Ö. Uzun, S. Arikan-Akdagli, The Emergence of Echinocandin-Resistant Candida glabrata Exhibiting High MICs and Related FKS Mutations in Turkey. *J Fungi (Basel)* **7** (2021).

121. F. Chapeland-Leclerc, C. Hennequin, N. Papon, T. Noël, A. Girard, G. Socié, P. Ribaud, C. Lacroix, Acquisition of flucytosine, azole, and caspofungin resistance in Candida glabrata bloodstream isolates serially obtained from a hematopoietic stem cell transplant recipient. *Antimicrob. Agents Chemother.* **54**, 1360–1362 (2010).

122. S. D. Singh-Babak, T. Babak, S. Diezmann, J. A. Hill, J. L. Xie, Y.-L. Chen, S. M. Poutanen, R. P. Rennie, J. Heitman, L. E. Cowen, Global analysis of the evolution and mechanism of echinocandin resistance in Candida glabrata. *PLoS Pathog.* **8**, e1002718 (2012).

123. Z. F. Al-Baqsami, S. Ahmad, Z. Khan, Antifungal drug susceptibility, molecular basis of resistance to echinocandins and molecular epidemiology of fluconazole resistance among clinical Candida glabrata isolates in Kuwait. *Sci. Rep.* **10**, 6238 (2020).

124. F. Winston, C. Dollard, S. L. Ricupero-Hovasse, Construction of a set of convenient Saccharomyces cerevisiae strains that are isogenic to S288C. *Yeast* **11**, 53–55 (1995).

Acknowledgments: We thank Anna Fijarczyk, François D. Rouleau and Stéphane Larose for bioinformatic assistance, Jordan Jalbert-Ross with technical assistance on preliminary assays, Philippe C. Després, François D. Rouleau and Soham Dibyachintan for critical reading of the manuscript and the whole team for feedback and emotional support on a regular basis throughout the project.

Funding:

Canadian Institutes of Health Research (CIHR) (Foundation grant 387697, CRL)

Genome Canada and Genome Quebec (grant 6569, CRL)

Canada Research Chair in Cellular Systems and Synthetic Biology (CRL)

Natural Sciences and Engineering Research Council of Canada (NSERC) (Grant RGPIN-2022-04721, PL)

Fonds de Recherche du Québec - Santé (FRQS) postdoctoral fellowship (RD)

NSERC postdoctoral fellowship (RD)

Author contributions:

Conceptualization: RD, AGT, CRL, PL

Methodology: RD, AGT, MG, AP, AKD, CRL, PL

Software: RD, AGT, MG, AP

Validation: RD, AGT, MG, AP, AKD

Formal analysis: RD, AGT, MG, AP

Investigation: RD, AGT, MG, AP, AKD

Resources: CRL, PL

Data curation: RD, AGT, MG, AP

Writing - Original draft: RD, AGT, MG

Writing - Review and editing: RD, AGT, CRL, PL

Visualization: RD, AGT, MG, AP

Supervision: RD, AGT, AP, AKD, CRL, PL

Project administration: CRL, PL

Funding acquisition: CRL, PL

Competing interests: Authors declare that they have no competing interests.

Data and materials availability: All data are available in the main text or the supplementary materials. Sequencing data are available at the NCBI Sequence Read Archive (SRA) under BioProject PRJNA1126009: http://www.ncbi.nlm.nih.gov/bioproject/1126009. All data and code to reproduce results and figures for the DMS and the machine learning sections are available at https://github.com/Landrylab/Durand_et_al_2024. All strains listed in S2 Data are available and can be requested by email at christian.landry@bcm.ulaval.ca.

Supplementary Materials

Materials and Methods

Supplementary Text

Figs. S1 to S17

Table S1

References (*29–124*)

Data S1 to S3

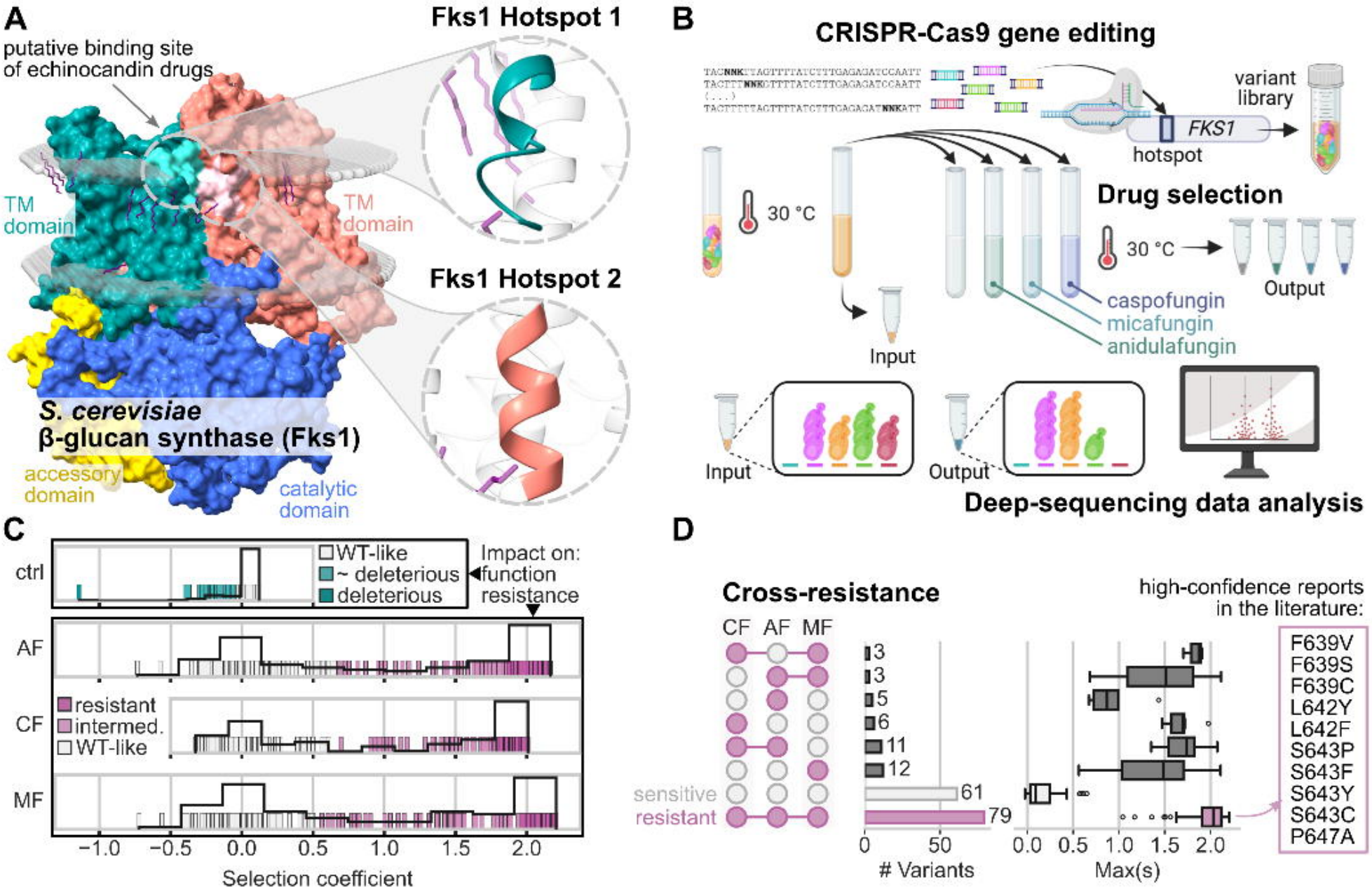
A
putative binding site
of echinocandin drugs
Fks1 Hotspot 1
Fks1 Hotspot 2
TM
domain
TM
domain
S. cerevisiae
β-glucan synthase (Fks1)
accessory
domain
catalytic
domain
B
CRISPR-Cas9 gene editing
variant
library
FKS1
hotspot
30 °C
Drug selection
30 °C
Output
caspofungin
micafungin
anidulafungin
Input
Input
Output
Deep-sequencing data analysis
C
ctrl
AF
CF
MF
WT-like
~ deleterious
deleterious
Impact on:
function
resistance
resistant
intermed.
WT-like
−1.0
−0.5
0.0
0.5
1.0
1.5
2.0
Selection coefficient
D
Cross-resistance
CF AF MF
sensitive
resistant
3
3
5
6
11
12
61
79
0
50
Variants
0.0 0.5 1.0 1.5 2.0
Max(s)
high-confidence reports
in the literature:
F639V
F639S
F639C
L642Y
L642F
S643P
S643F
S643Y
S643C
P647A

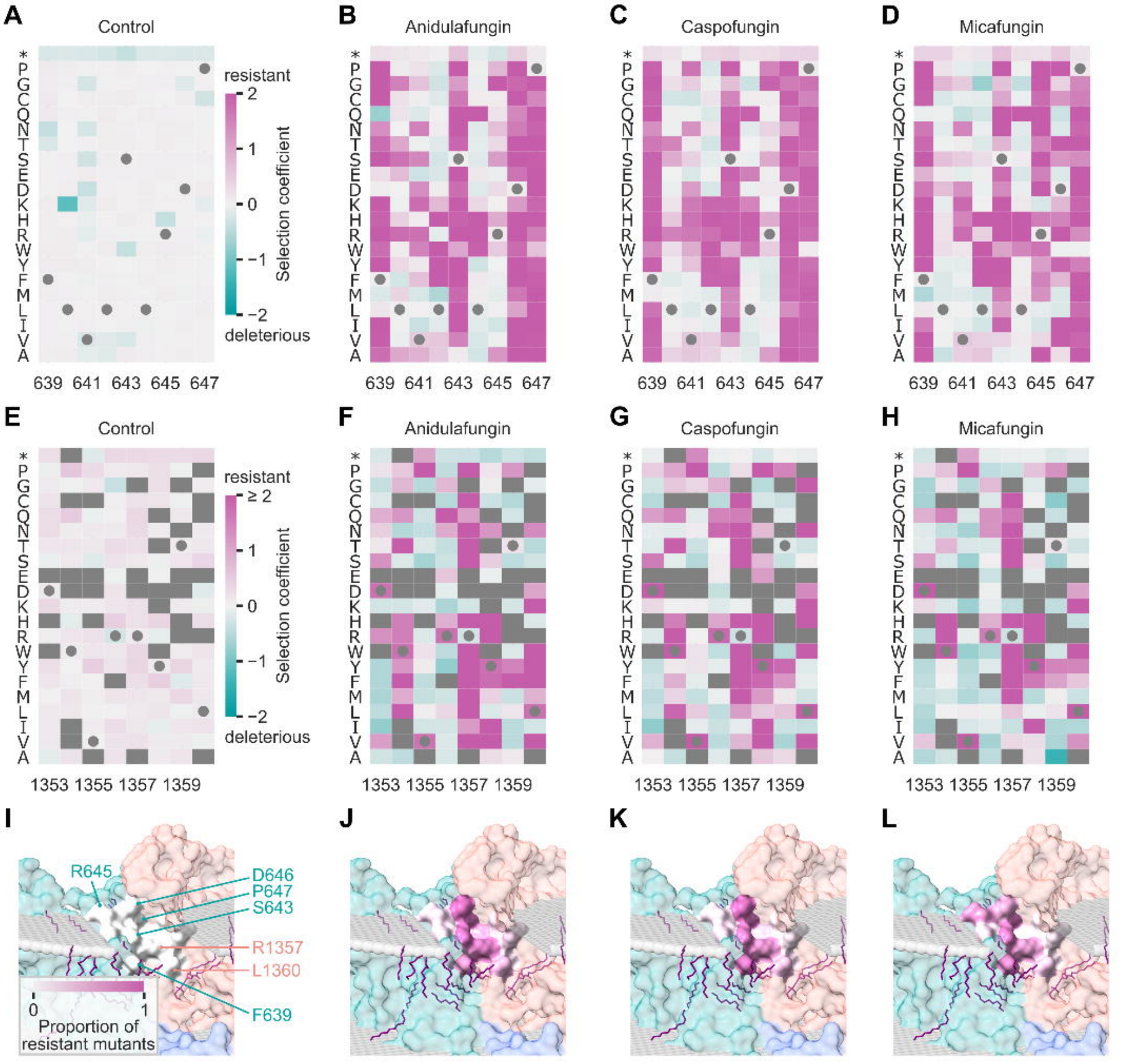
A
Control
B
Anidulafungin
C
Caspofungin
D
Micafungin
resistant
Selection coefficient
deleterious
639 641 643 645 647
E
Control
F
Anidulafungin
G
Caspofungin
H
Micafungin
1353 1355 1357 1359
I
J
K
L
R645
D646
P647
S643
R1357
L1360
F639
Proportion of resistant mutants

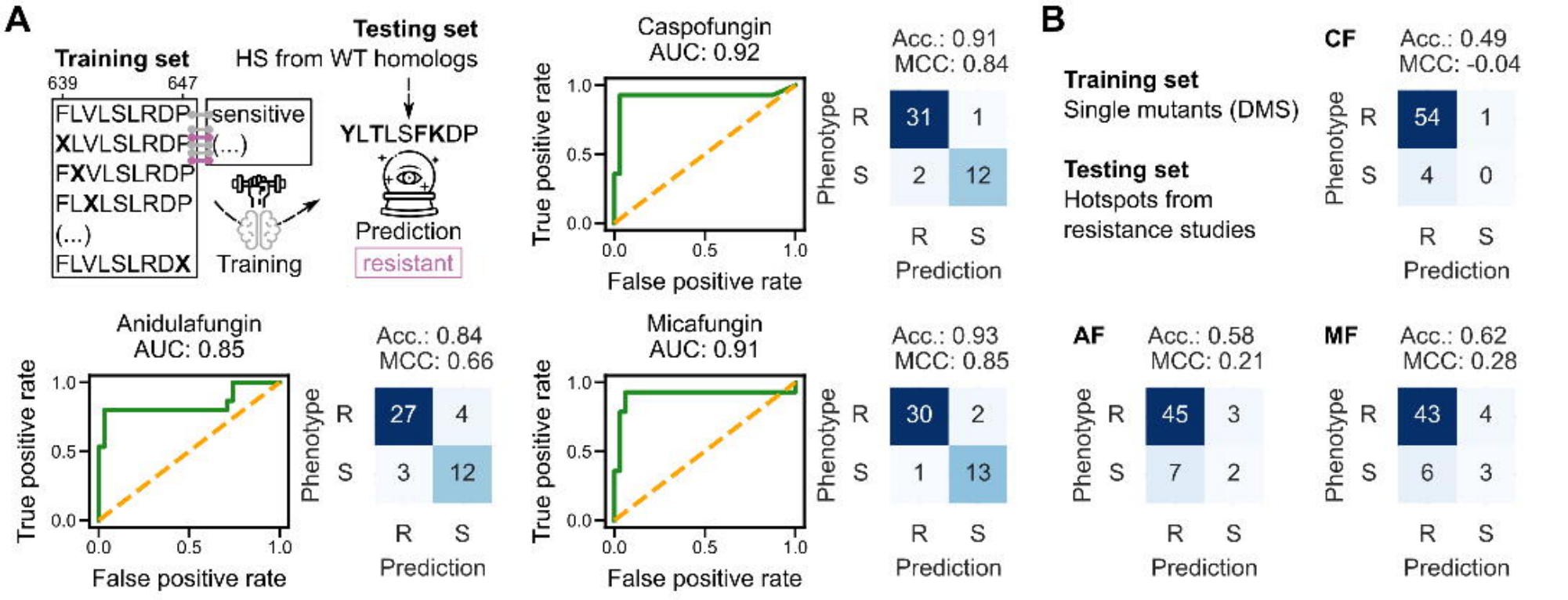
A
Training set
639
647
FLVLSLRDP
XLVLSLRDP
FXVLSLRDP
FLXLSLRDP
(...)
FLVLSLRDX
sensitive
(...)
Training
Testing set
HS from WT homologs
YLTLSFKDP
Prediction
resistant
Caspofungin
AUC: 0.92
Acc.: 0.91
MCC: 0.84
True positive rate
False positive rate
Phenotype
R
S
31
1
2
12
Prediction
Anidulafungin
AUC: 0.85
Acc.: 0.84
MCC: 0.66
27
4
3
12
Micafungin
AUC: 0.91
Acc.: 0.93
MCC: 0.85
30
2
1
13
B
Training set
Single mutants (DMS)
Testing set
Hotspots from
resistance studies
CF
Acc.: 0.49
MCC: -0.04
54
1
4
0
AF
Acc.: 0.58
MCC: 0.21
45
3
7
2
MF
Acc.: 0.62
MCC: 0.28
43
4
6
3

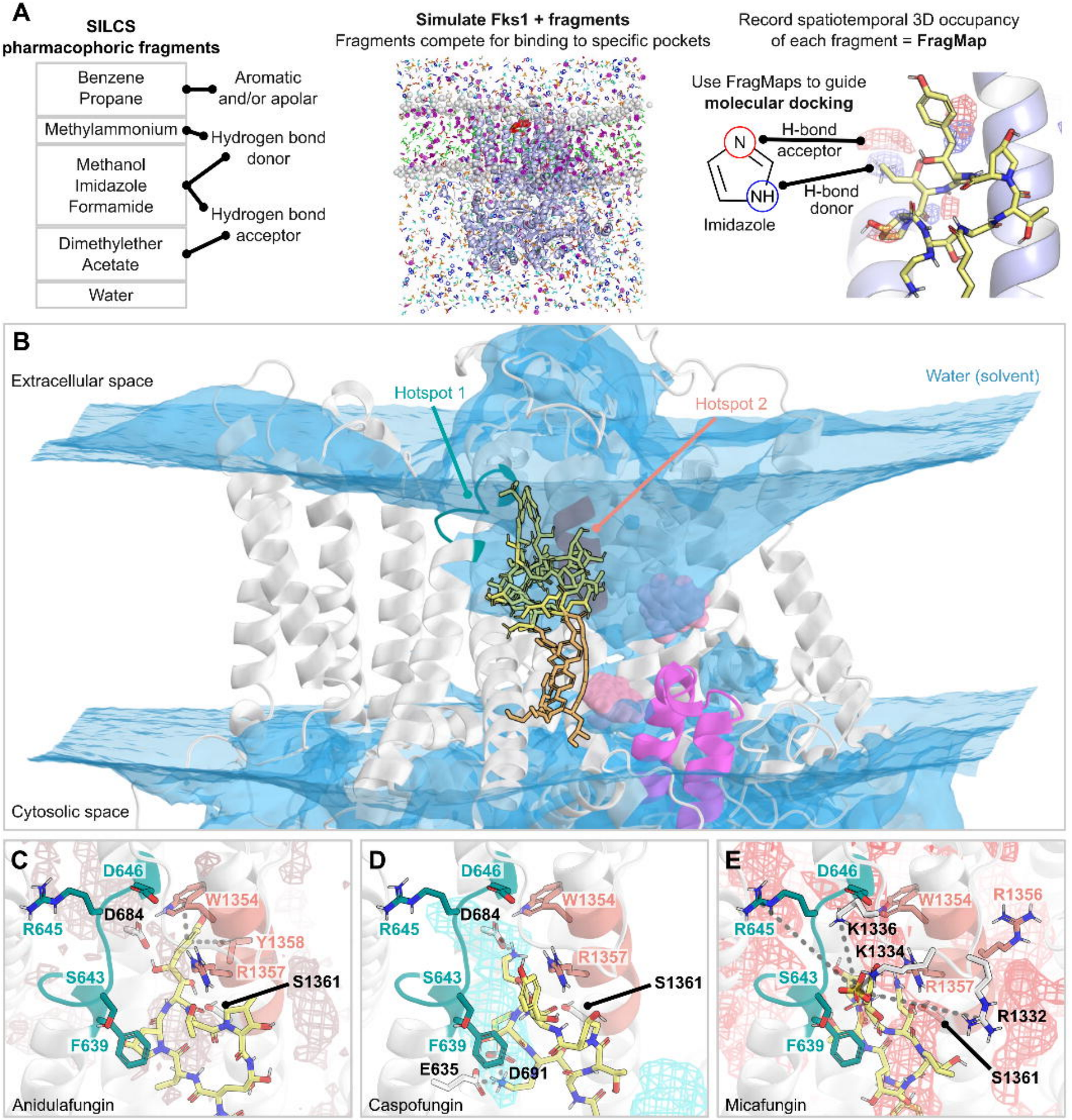
A
SILCS
pharmacophoric fragments
Benzene
Propane
Aromatic
and/or apolar
Methylammonium
Hydrogen bond
donor
Methanol
Imidazole
Formamide
Hydrogen bond
acceptor
Dimethylether
Acetate
Water
Simulate Fks1 + fragments
Fragments compete for binding to specific pockets
Record spatiotemporal 3D occupancy
of each fragment = FragMap
Use FragMaps to guide
molecular docking
N
NH
H-bond
acceptor
H-bond
donor
Imidazole
B
Extracellular space
Hotspot 1
Hotspot 2
Water (solvent)
Cytosolic space
C
D646
R645
D684
W1354
Y1358
R1357
S643
S1361
F639
Anidulafungin
D
D646
R645
D684
W1354
R1357
S643
S1361
F639
E635
D691
Caspofungin
E
D646
R645
K1336
K1334
W1354
R1356
R1357
S643
R1332
F639
S1361
Micafungin

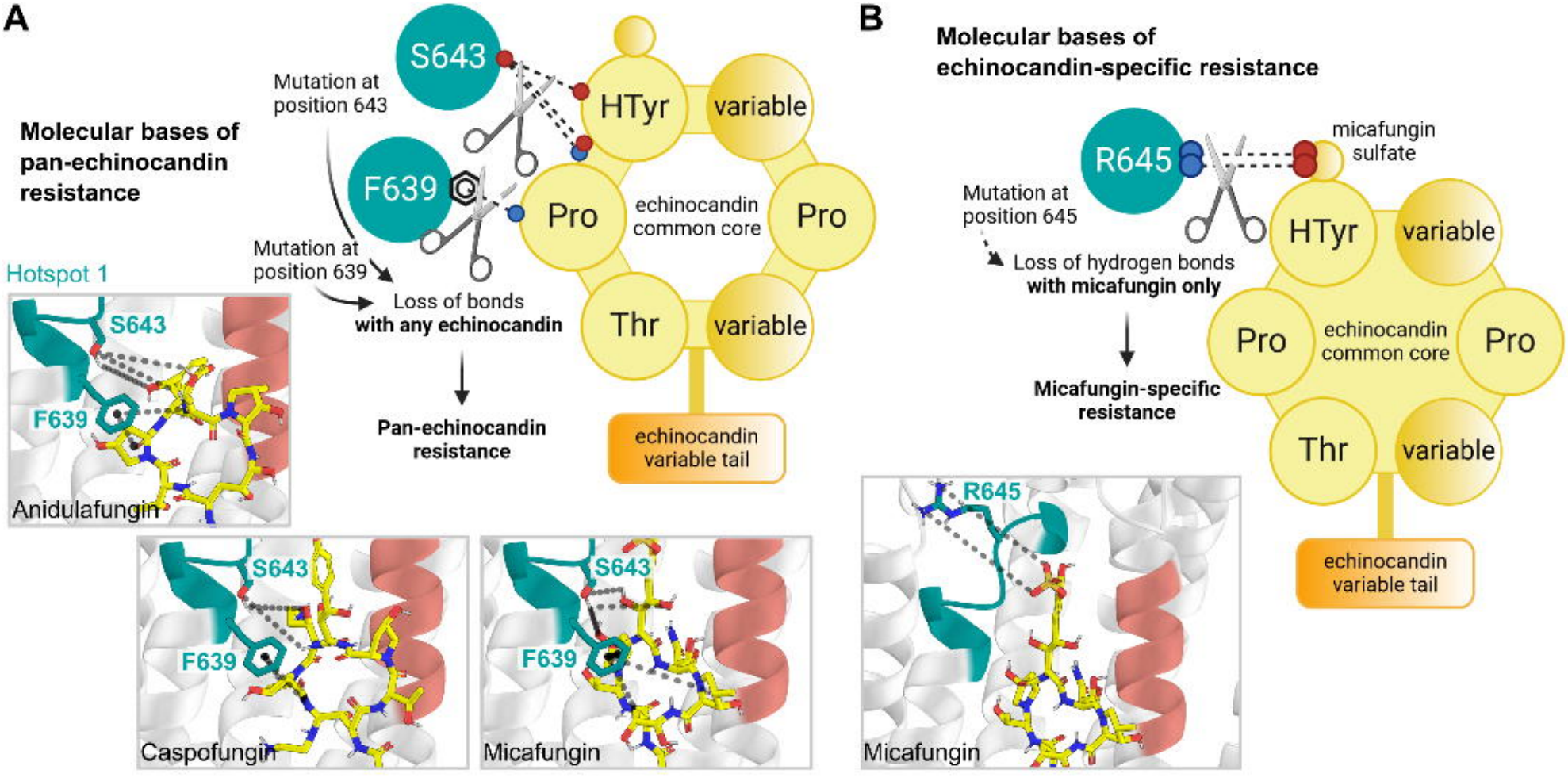
A
Molecular bases of pan-echinocandin resistance
S643
F639
Mutation at position 643
Mutation at position 639
Loss of bonds with any echinocandin
Pan-echinocandin resistance
HTyr
variable
Pro
echinocandin common core
Pro
Thr
variable
echinocandin variable tail
Hotspot 1
S643
F639
Anidulafungin
S643
F639
Caspofungin
S643
F639
Micafungin
B
Molecular bases of echinocandin-specific resistance
R645
micafungin sulfate
Mutation at position 645
Loss of hydrogen bonds with micafungin only
Micafungin-specific resistance
HTyr
variable
Pro
echinocandin common core
Pro
Thr
variable
echinocandin variable tail
R645
Micafungin